FRACTAL AND DENDRITIC GROWTH OF SURFACE AGGREGATES

H. BRUNE, K. BROMANN, and K. KERN
Institut de Physique Expérimentale, EPFL, CH-1015 Lausanne, Switzerland

J. JACOBSEN, P. STOLTZE, K. JACOBSEN, and J. NØRSKOV
Center for Atomic-scale Materials Physics and Physics Department
Technical University of Denmark, DK-2800 Lyngby, Denmark

ABSTRACT

The similarity of patterns formed in non-equilibrium growth processes in physics, chemistry and biology is conspicuous and many attempts have been made to discover common mechanisms underlying their growth. The central question in this context is what causes some patterns to be dendritic, as e.g. snowflakes, while others grow fractal (randomly ramified). Here we report a crossover from fractal to dendritic patterns for growth in two dimensions: the diffusion limited aggregation of Ag atoms on a Pt(111) surface as observed by means of variable temperature STM. The microscopic mechanism of dendritic growth can be analyzed for the present system. It originates from the anisotropy of the diffusion of adatoms at corner sites which is linked to the trigonal symmetry of the substrate. This corner diffusion is observed to be active as soon as islands form, therefore, the classical DLA clusters with the hit and stick mechanism do not form. The ideas on the mechanism for dendritic growth have been verified by kinetic Monte-Carlo simulations which are in excellent agreement with experiment.

INTRODUCTION

In the "classical" Diffusion Limited Aggregation (DLA) computer codes, clusters are formed as randomly diffusing particles stick irreversibly to the perimeter of a growing aggregate **[1-3]**. These models always produce *randomly ramified* aggregates, no matter whether they are carried out on a lattice or not (off-lattice DLA) **[3, 4]**. Nonequilibrium aggregation processes in nature, however, quite often result in *dendritic* patterns which are characterized by preferred growth directions **[5-7]**. Despite a considerable theoretical effort, the relationship between ordered and randomly ramified patterns has not yet been solved **[8, 9]**. Both objects have a fractal dimension close to 1.7 **[10, 11]**, but their different shape is evident for the unaided eye (compare e.g. Figs. 1 and 2 below).

It is generally accepted that the key to dendritic growth is anisotropy **[12-15]**. This can either be linked to the symmetry of the aggregating particles themselves, which is then amplified to the overall pattern shape as the aggregate grows (a well known example for this is the snowflake **[16]**), or it can be due to the symmetry of the underlying substrate. Examples for this are given in Fig. 2 below, where we observe dendritic growth for two-dimensional metal aggregation on three hexagonally close packed substrates.

In order to reproduce dendritic structures basically two approaches have been followed to modify the hit and stick mechanism in DLA-models. One is the introduction of curvature dependent sticking probabilities **[17]** and the second noise reduction, where atoms are only attached if the approached site has been visited m-1 times before **[18]**. Both mechanisms are, however, irrelevant for low temperature metal epitaxy, since there the sticking probability is 1 and independent of curvature.

In the first metal deposition experiments carried out with the STM (at 300K), ramified growth and irregular island shapes were reported **[19-21]**. In particular, the Au aggregates on Ru(0001) have been considered as an example for classical DLA because of their fractal dimension **[21]**. However, it had been realized later that their branch width (100-200Å) points to a considerable amount of edge diffusion **[22-25]**. Similarly, the first results reported for lower temperature, showing ramified islands for homoepitaxy on Pt(111), were also interpreted as the physical realization of the hit and stick mechanism **[26]**.

The first time dendrites have been reported, and their distinction to randomly ramified aggregates was made clear, was for the aggregation of Ag on Pt(111) **[11, 27, 28]**. These

Mat. Res. Soc. Symp. Proc. Vol. 407 © 1996 Materials Research Society

results have inspired simulations which were very successful in reproducing island densities **[29, 30]**. However, they assume a hit and stick mechanism and neglect the specific substrate symmetry (which both holds for aggregation of much bigger clusters **[31]**) and therefore are not suited to simulate dendritic growth. The same is true for most of the models that study metal nucleation. since they were carried out on a square lattice **[23, 32-34]**. Those Kinetic Monte-Carlo (KMC) simulations which have been performed on a hexagonal lattice either focused on the shape of compact islands on Pt **[35, 36]**, or they do not distinguish between the two types of close packed steps present on a hexagonal substrate **[22, 37]**. There are close packed {111}-facets and more open {100}-facets (see vacancy islands in Fig. 3 and model in Fig. 4). They have been called B- and A-steps, respectively **[38]**.

Thus to date, a realistic description of the atomic processes leading to dendritic growth in metal aggregation on hexagonal substrates was lacking. We will present a microscopic model explaining dendrite formation and discuss the importance of the different relaxation processes at the island edge and their influence on the aggregate's shape.

EXPERIMENTAL

The experiments have been performed with a variable-temperature STM mounted in UHV, which operates in the temperature range from 25K to 800K (for experimental setup see e.g. ref. **[28]**). The Pt(111) crystal has been cleaned by repeated cycles of Ar ion bombardment (650eV) at 830K, annealing in oxygen atmosphere (880K, $1x10^{-7}$ mbar) and subsequent flash to 1300K. The Ag (purity 99.995%) aggregates were grown by vapor-phase epitaxy with an MBE-Knudsen-cell at a background pressure better than $2x10^{-10}$ mbar. The STM images have been measured in the constant current mode. All images shown here were recorded in differential mode, which means that the derivative $\partial z/\partial x$ of the lines of constant tunnel current is recorded. They therefore appear as illuminated from the left. The images are not corrected for thermal drift and have not been filtered.

RESULTS

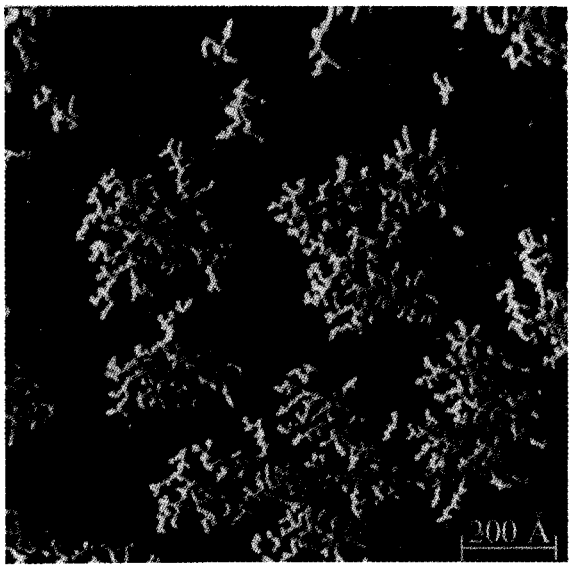

Fig. 1: Fractal Ag aggregates grown on Pt(111) at 110K and extremely low deposition flux of F = $1.6x10^{-5}$ML/s (1200Å x 1200Å, coverage Θ = 0.12ML).

The two-dimensional Ag aggregates shown in Fig. 1 have been grown at 110K. The coverage of 0.12 monolayers has been deposited at an extremely low Ag flux of 1.6×10^{-5} ML/s. Under these conditions, large clusters (~3000 Ag atoms) with an open ramified structure are formed. The branches of the clusters frequently alter their direction of growth and thus show no long range correlation with the symmetry axes of the substrate. The branch thickness is almost constant over the entire aggregate and much smaller than its radius of gyration. In fact the arms are only 2±1 atoms wide as determined from the total arm length and the cluster size. (Branches are imaged (14±1)Å wide in Fig. 1, which is consistent with their actual width if the finite curvature of the STM-tip is taken into account.) The shape of the Ag aggregates grown at 110K is very similar to that of fractal aggregates simulated with the classical DLA computer codes. However, for aggregation on hexagonal substrates, these patterns are the exception rather than the rule.

Patterns formed by the aggregation of Ag at moderate growth speeds on three hexagonally close packed metal surfaces, i.e. the (111) surfaces of Pt, Ag, and one Ag monolayer pseudomorphically adsorbed on Pt(111) **[39]**, all have in common a nice dendritic shape (see Fig. 2). The variable temperature STM images show that their branches preferentially grow into three directions, which are rotated by 120° with respect to each other. As will become evident from Fig. 3 below, they are the crystallographic $\langle \bar{1}\bar{1}2 \rangle$-directions which are perpendicular to A-steps, one of them has been labeled A.

For the first case of Ag/Pt(111) (Fig. 2A) the trigonal symmetry of the aggregate is best seen from its triangular envelope, but also the longest central branches clearly point into the preferred growth directions. Notice also that the material attached to the straight substrate step in the lower part of the image does not grow perpendicular to the edge (which would be the B-direction since this step is a {111}-facet, i.e. of B-type) but instead in two of the A-directions forming angles of ±30° with respect to the step. At 80K islands are too small to branch more than once and the growth anisotropy leads to equally oriented Y's (inset Fig. 2A). For Ag/Ag(111) (Fig. 2B) the preferred growth in three directions is clearly seen from of the central branches of the aggregates. The trigonal symmetry of the aggregates on one pseudomorphic Ag layer is even more pronounced. Their shape resembles very much that of needle crystals, which are the extreme case of anisotropic growth **[40]**. These examples strongly suggest that dendritic growth is common for low temperature metal aggregation on hexagonally close packed metal surfaces at usual growth rates. In fact also Pt islands formed at low T seem to have dendritic shapes with preferential growth in A-direction **[41]**.

In order to analyze the atomistic process responsible for the formation of dendrites on hexagonal surfaces, we will distinguish between two diffusion processes that can take place at the island edge. Depending on whether an adatom starts from a site which is laterally *two-* or *one-fold* coordinated to the island, i.e. whether the initial site is an edge or a corner, we will call its displacement *edge-* or *corner*-diffusion, respectively **[42]**. For corner diffusion the final coordination can be 1 or 2. For edge diffusion the final coordination is 2. The case where an edge atom (2-fold coordinated) goes to a corner (1-fold) becomes important at higher temperatures, and should be treated separately.

It turns out that this distinction is rather useful since these processes have quite different effects on the aggregate's shape. Edge diffusion leads to a thickening of the aggregates' branches **[22-25]**. Closer inspection of the dendrites in Fig. 2 indeed reveals that the branches become thicker in going from images (A) to (C) (notice the different scale). From the narrow branches for Ag on Pt(111) in Fig. 2A (2±1 atoms wide) we can deduce that edge diffusion is practically frozen (at 130K and the applied deposition flux) **[25]**. Edge diffusion is active for Ag/Ag(111) at 110K, since branches are 8±1.5 atoms wide **[25]** (Fig. 2B). It is even more involved in the case of Ag/1MLAg/Pt(111) leading to 18±3 atoms wide branches (Fig. 2C). From the fact that dendritic growth occurs in all examples shown in Figure 2, independent from the amount to which edge diffusion is involved, we can argue that it is very unlikely to be the origin of dendritic growth **[43]**.

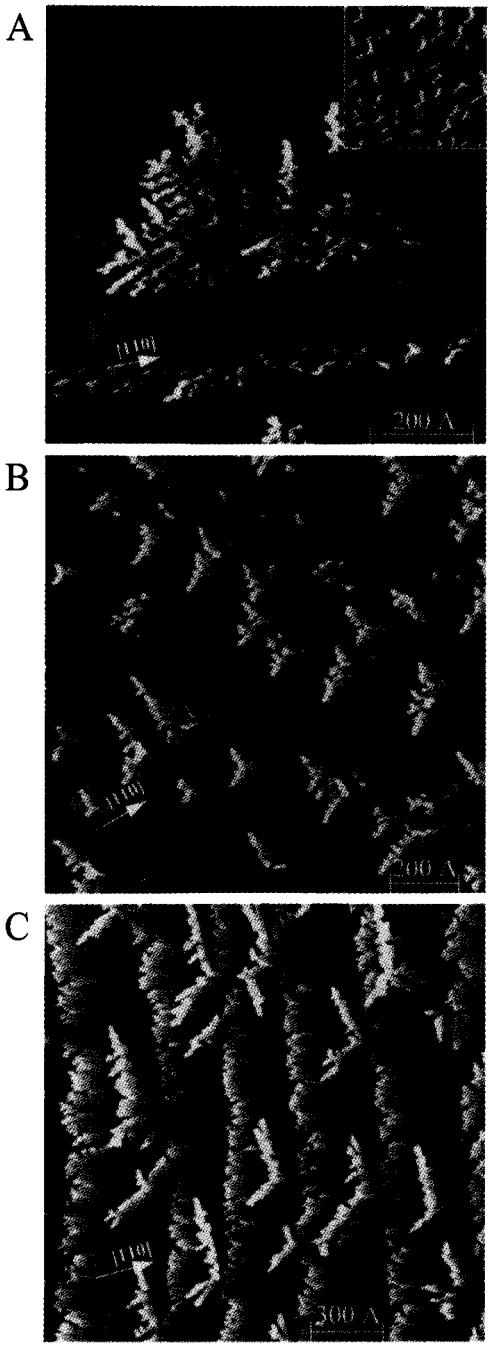

Fig. 2: Dendritic patterns form for deposition of Ag onto Pt(111) at 130K (**A**) and 80K (inset), onto Ag(111) at 110K (**B**), and on a pseudomorphic monolayer of Ag adsorbed on Pt(111) at 170K (**C**). The STM topographs have been recorded isothermally to deposition and show the surface as it appears when illuminated from the left. The Ag coverage is Θ = 0.12ML, the deposition flux F = $1.1 \times 10^{-3} ML s^{-1}$.

In order to proceed further in our analysis we identify the crystallographic directions in which branching preferentially occurs in the experiment (see Fig. 3). One way to calibrate the crystallographic directions on a hexagonal substrate is to create vacancy islands with the thermodynamic equilibrium shape **[44]**. These quasi hexagons are bound by 6 monoatomic steps running in the close packed $\langle 1\bar{1}0 \rangle$-directions. They devide up into B- and A-type steps opposing each other. Due to their lower free energy, the first ($\{111\}$-facets) are the long sides of the hexagons, while the latter ($\{100\}$-facets) form the short ones. Ag has been deposited at 100K onto a substrate where these vacancy island mark the crystallographic directions. At this temperature, the aggregates obey Y-shape for the same reason as at 80K (inset in Fig. 2A), they are too small to branch more than once. Their branches are oriented exclusively into the $\langle \bar{1}\,\bar{1}2 \rangle$-directions, i.e. perpendicular to A-steps, which are also the preferred growth directions for the bigger aggregates shown above (Fig. 2).

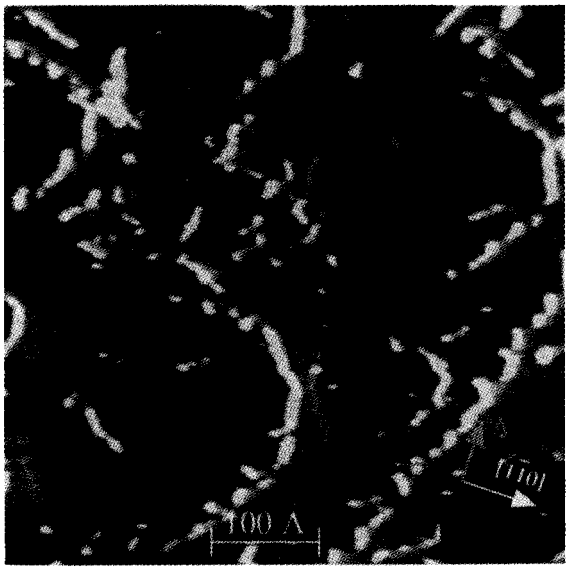

Fig. 3: The anisotropic growth leads to small Y-shaped dendrites for Ag on Pt(111) at 100K. Removal of about 0.5ML of the Pt(111) substrate by sputtering (600K) and subsequent annealing (700K) creates equilibrium vacancy islands. They serve as calibration for the two different crystallographic directions labeled A for $\langle \bar{1}\,\bar{1}2 \rangle$, and B for $\langle 11\bar{2} \rangle$, respectively. It is evident that the branches of these Y's exclusively grow into A-directions, i.e., perpendicular to A-steps.

In order to get insight into the relaxation processes at the aggregate's perimeter we have calculated diffusion barriers with Effective Medium Theory (EMT) **[45, 46]**. The results show that for all three cases where we found dendritic growth in the STM experiment, corner diffusion to an A-step has a much lower barrier than displacement from a corner to a B-step (Fig. 4 and Table 1). This asymmetry can be rationalized from simple geometric reasons. From inspection of the model in Fig. 4 it becomes evident that displacement from a corner to an A-step can be done via an hcp-hollow site without loosing the coordination to the heptamer, whereas for diffusion towards a B-step the hcp-site is situated too close towards the island. Thus the adatom has to walk almost over an on-top site, which is much more costly in energy.

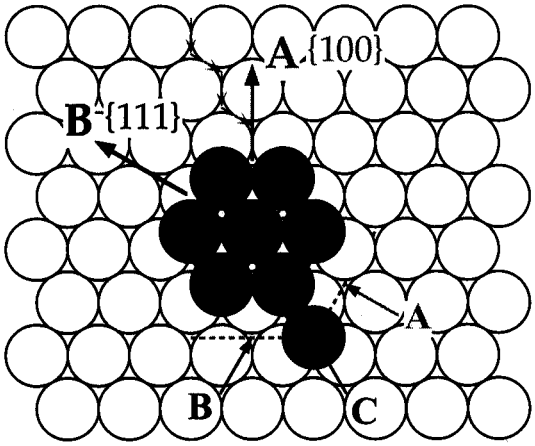

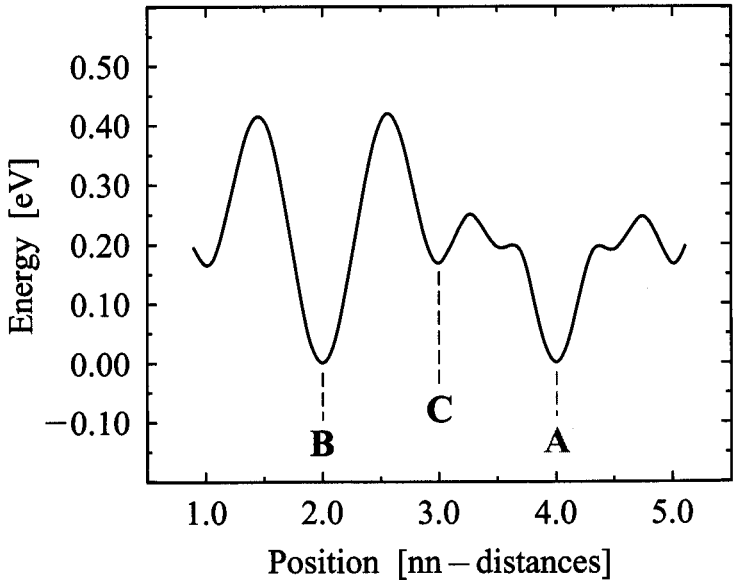

Fig. 4: Difference in total energy of a Ag adatom diffusing around a Ag heptamer on Pt(111) as calculated with EMT (A- and B-directions are indicated in the ball model). The diffusion processes with the lowest barriers evidently are that from a corner (C) and the hcp-site close to it to an A-step.

For some systems like Pt(111) **[36]** and Au(111) homoepitaxy, the corner asymmetry is less pronounced in the EMT-calculations and the direction is even inverted, i.e., displacement to B-steps is slightly preferred (Pt: E_{Ac}/E_{Bc} = 212meV/173meV, Au: E_{Ac}/E_{Bc} = 146meV/101meV).

Therefore, it is important to notice that there is a second anisotropy which generally holds for hexagonally close packed surfaces. An atom that diffuses towards an A-step close to a corner does this via the hcp-site located between the two fcc-sites at the corner and the A-step (ball model Fig. 4). Already at this point, it feels the two-fold coordination at the step and has a much lower barrier to go there than to diffuse to the corner site (see asymmetry in activation energy around the hcp-site and the flashes indicating an approaching atom in Fig. 4). On a B-step, the decision whether the atom goes to the corner or the step is made much earlier so that it is not guided to the step.

Both these asymmetries give a significant preference in populating A-steps. It is important to note that both diffusion processes, i.e., corner to A-step and that from the hcp-site to an A-step, have an activation energy comparable to, or even below, that obtained for terrace diffusion. Therefore, relaxation towards A-steps is active as soon as nucleation and aggregation set in, and the classical hit and stick DLA cluster do not form. The barriers for the more difficult corner process (corner-to-B step), and those for edge diffusion, as well as to escape from an edge to a corner, are significantly higher, which implies that these processes can be frozen at low temperatures.

Let us now see how this specific preference for A-steps decides on the shape of the growing aggregate. We assume to start from a tetramer which is bound by two A- and B-steps. Atoms impinging at corners adjacent to an A-step, as well as those approaching the A-step at the two neighboring hcp-sites, will end up at the A-step, which significantly increases the probability of attachment there. Once the atoms are at A-steps, they form a protruding tip and thus have a slightly higher capture rate than straight steps. This is known as "tip-effect" or Mullins Sekerka instability **[2, 47]**. Atoms arriving at such an atomic "tip", can diffuse force and back between the two corner sites but they cannot escape from there, since this would be diffusion to the adjacent B-steps, which is frozen. If a second atom arrives at the respective free corner, a new A-step is formed, which then again collects very effectively diffusing atoms and growth in the A-direction proceeds. If the atom arrives such that a linear chain in the close packed direction would be formed, the EMT calculations suggest that these chains can relax with a low energy barrier to a more compact form which also ends with an A-step. Therefore, growth of Y's occurs as A-steps effectively capture atoms, these atoms form tips which are traps for attaching atoms due to the frozen corner-to-B diffusion. Atoms attached there thus stay until a partner arrives to form a dimer which provides new A-steps. Direct attachment to B-steps leads to statistical deviations from this behavior. However, it also creates new A-steps which can be the origin for a new branch in the preferred A-directions.

Table 1: Energy barriers for the most relevant atomic diffusion processes involved in metal aggregation on hexagonal substrates for the systems studied in Figs. 1 and 2 (E_m stands for terrace diffusion, E_{Ac} for corner-to-A-step, E_{Bc} for corner-to-B-step, E_{Ae} and E_{Be} denote A- and B-edge diffusion). The experimental values for terrace diffusion have been obtained by the analysis of the saturation island density as a function of T at a critical cluster size of 1 **[48, 49]**. (* in Fig. 4D E_{Bc} has been lowered, ** E_m has been lowered for 130K in order to account for dimer instability at this temperature, see text.)

Ag diffusion on substrates:	E_m [meV] STM	E_m [meV] EMT	E_{Ac}/E_{Bc} EMT	E_{Ae}/E_{Be} EMT	E_{Ac}/E_{Bc} KMC	E_m [meV] KMC
Pt(111)	157±10	80	80/248	187/389	160/500 160/320*	160 120**
Ag(111)	97±10	67	73/139	222/300	—	—
1MLAg/Pt(111)	60±10	50	39/165	167/354	—	—

To test the ideas on the mechanism for dendritic growth we performed Kinetic Monte-Carlo (KMC) simulations (the KMC-program has been described in ref. **[36]**) for Ag/Pt(111) on a hexagonal lattice where we distinguish between A- and B-directions (see Fig. 5). Activation energies on surfaces are often underestimated by the EMT. However, the EMT generally gives a

good idea on the energetic hierarchy of different diffusion processes. Therefore, as a first input for the KMC we use the EMT activation energies scaled by a common factor of 2, since then the barrier for terrace diffusion equals the experimental value of E_m = 160meV **[48]**. All prefactors have been set to the experimental value for terrace diffusion of $1x10^{13}s^{-1}$. Using E_m = 160meV in a KMC simulation nicely reproduces the experimental island densities at temperatures up to 110K, where dimers are stable and immobile. In our simulations done at 130K, we have used E_m = 120meV as an effective barrier for terrace diffusion which then also accounts for the dimer instability or mobility. This way, we again get the experimental island density at 130K and thus the correct lateral impinging rate of atoms to each island.

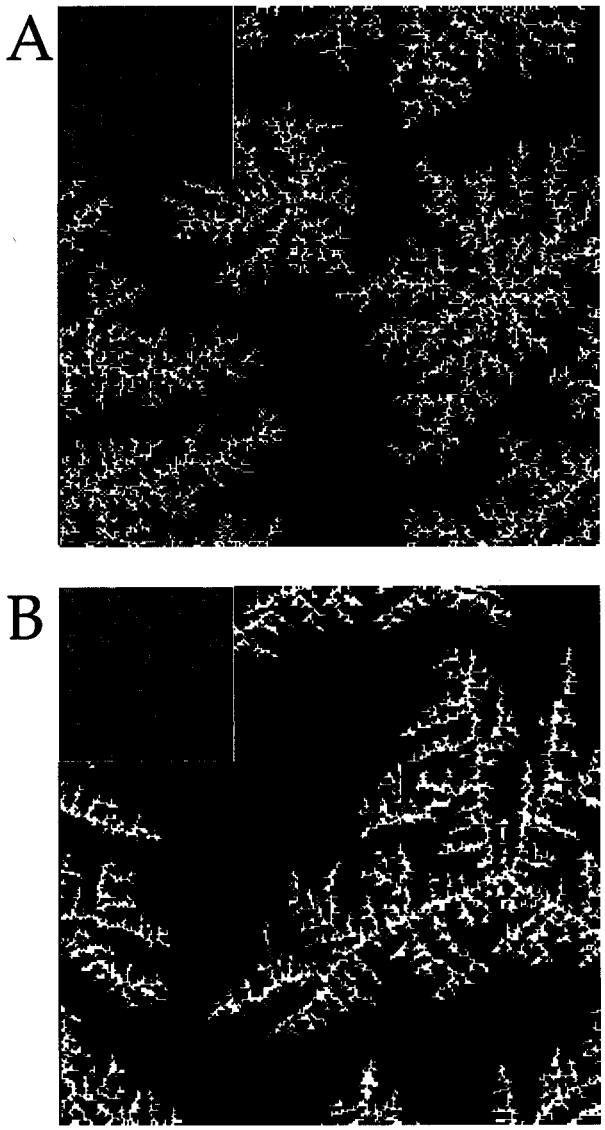

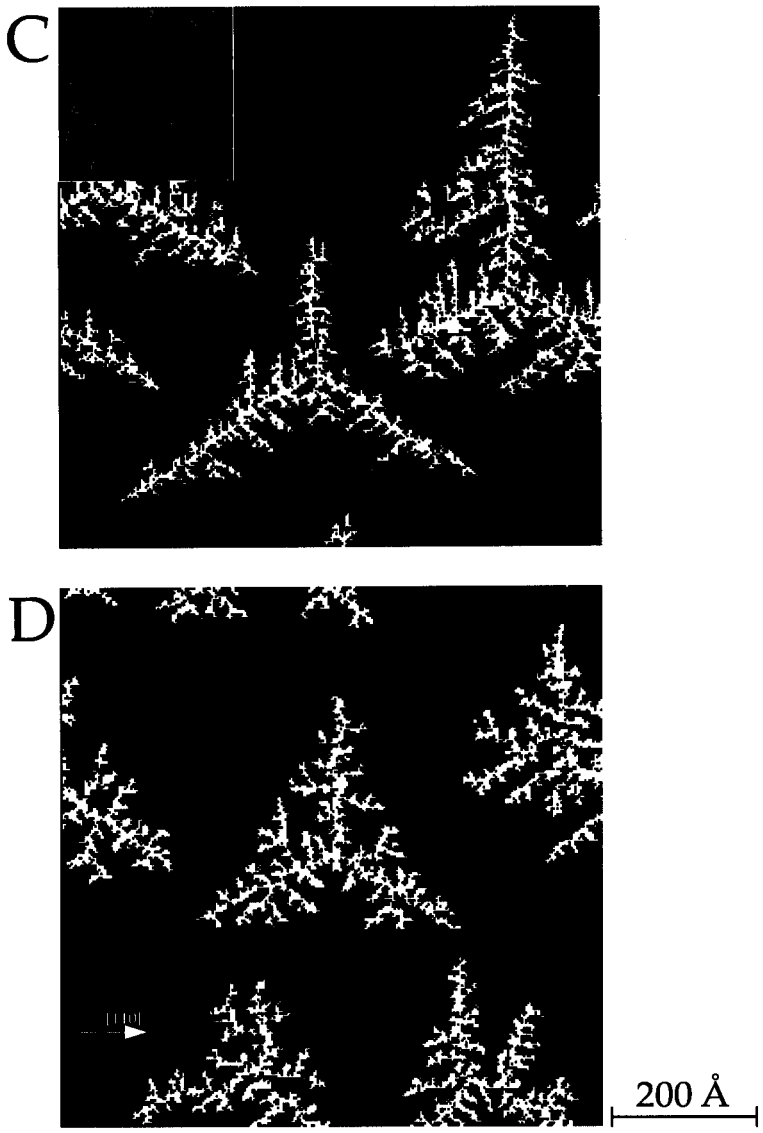

Fig. 5: KMC simulations of the STM experiments for Ag/Pt(111). As in Fig. 2A, the scale is the same for figures and insets, they correspond to growth temperatures of 130K and 80K, respectively. Coverages and deposition rates are as in the experiment. For hit and stick, classical DLA fractals result (**A**). The key process for dendritic islands is diffusion from corner to A-steps (**B**). Close packed chains that occasionally form in (B) are no more observed when a small atomic row is allowed to relax (**C**). Best agreement with experiment is obtained when corner to B-step diffusion is introduced (**D**).

The KMC simulations shown in Fig. 5 nicely illustrate the influence of the different processes on the island shape. The hit and stick case, where terrace diffusion and jump down from island tops are the only atomic displacements allowed, gives the classical randomly ramified DLA fractals where the substrate symmetry is not visible in the overall cluster shape (Fig. 5A). Turning on corner diffusion towards A-steps induces a marked change towards trigonal symmetry with branches predominantly growing into A-direction (Fig. 5B). However the aggregates form monoatomic chains along $\langle 1\bar{1}0 \rangle$ and the Y-shaped islands experimentally observed at 80K cannot be reproduced (see inset in Fig. 5B) . If we introduce further the collective relaxation of these chains, we can improve this. The scaled EMT barrier of E_{coll} = 240meV is too high for the process to happen sufficiently frequent at 80K, but choosing E_{coll} = 160meV we get a strikingly good agreement with the experimental island shapes at 130K and 80K (Fig. 5C and inset).

We want to point out that the important time scale for all relaxation processes at the island edge is the lateral impinging rate of diffusing atoms. The observed island shapes at 80K set an upper limit of 160meV for the barriers of the corner-to-A process and the collective relaxation of the $\langle 1\bar{1}0 \rangle$-chains. Speeding up these processes by reducing their energy barriers in the simulations would not significantly change the morphology of the obtained islands (Fig. 5B-D). Similarly, we find that the experimentally observed island shapes at 130K (Fig. 2A) set a lower limit of 320meV for the barrier of the corner-to-B process. The scaled EMT barrier of 500meV freezes this process completely even at 130K. In Fig. 5D, we show the result of a simulation using E_{Bc} = 320meV at 130K. This gives an even better agreement with the experimentally observed islands. There is still strongly preferred growth perpendicular to the A-steps, however, now the simulated islands bear some of the randomness characteristic of the experiment with occasional growth of the branches perpendicular to B-steps.

In general, the growth direction of the aggregate's branches is largely determined by corner diffusion. It decides whether randomly ramified or dendritic patterns will evolve, and determines the orientation of the latter. The branch width, on the other hand, is determined by edge diffusion, which has much less influence on their growth direction. Finally, compact islands can only be formed if atoms can leave the two-fold coordination at edges and diffuse around corners, a process which has a slightly higher barrier than edge diffusion.

CONCLUSIONS

In conclusion, we have presented STM experiments at low temperature showing that randomly ramified growth is the exception whereas dendritic growth is the rule for diffusion limited metal aggregation on three different hexagonal surfaces. The kinetic mechanism giving rise to the trigonal symmetry has been identified by using EMT energy calculations and kinetic Monte-Carlo simulations. The key process is the preferential diffusion of atoms from one-fold corner sites as well as from sites between a corner and a step towards A-steps. Both processes significantly increase the population of these steps and thereby promote dendritic growth. Since at least the latter is always present, dendritic growth is expected to be the rule for low temperature metal aggregation on hexagonally close packed substrates.

REFERENCES

[1] T. A. Witten and L. M. Sander, Phys. Rev. Lett. **47**, 1400 (1981).
[2] T. A. Witten and L. M. Sander, Phys. Rev. B **27**, 5686 (1983).
[3] P. Meakin, Phys. Rev. A **27**, 1495 (1983).
[4] J. P. Eckmann, P. Meakin, I. Procaccia and R. Zeitak, Phys. Rev. Lett. **65**, 52 (1990).
[5] D. Grier, E. Ben-Jacob, R. Clarke and L. M. Sander, Phys. Rev. Lett. **56**, 1264 (1986).
[6] Y. Sawada, A. Dougherty and J. P. Gollub, Phys. Rev. Lett. **56**, 1260 (1986).
[7] J. S. Langer, Rev. Mod. Phys. **52**, 1 (1980).
[8] M. B. Amer, P. Pelcé and P. Tabeling, *Growth and Form: nonlinear aspects* (Plenum Press, New York, 1991).
[9] H. Takayasu, *Fractals in the physical sciences* (Manchester University Press, Manchester, New York, 1990).
[10] P. Meakin, Phys. Rev. A **33**, 3371 (1986).
[11] H. Brune, C. Romainczyk, H. Röder and K. Kern, Nature **369**, 469 (1994).

[12] J. Nittmann and H. E. Stanley, J. Phys. Math. Gen. **20**, L981 (1997).
[13] A. Buka, J. Kertész and T. Vicsek, Nature **323**, 424 (1986).
[14] E. Ben-Jacob, R. Godbey, N. D. Goldenfeld, J. Koplik, H. Levine, T. Mueller and L. M. Sander, Phys. Rev. Lett. **55**, 1315 (1985).
[15] V. Horváth, T. Vicsek and J. Kertész, Phys. Rev. A **35**, 2353 (1987).
[16] J. Nittmann and H. E. Stanley, Nature **321**, 663 (1986).
[17] T. Vicsek, *Fractal Growth Phenomena* (World Scientific, Signapore, 1989).
[18] P. Meakin, Phys. Rev. A **36**, 332 (1987).
[19] D. D. Chambliss and R. J. Wilson, J. Vac. Sci. Technol. B **9**, 928 (1991).
[20] A. Brodde, G. Wilhelmi, D. Badt, H. Wengelnik and H. Neddermeyer, J. Vac. Sci. Technol. B **9**, 920 (1991).
[21] R. Q. Hwang, J. Schröder, C. Günther and R. J. Behm, Phys. Rev. Lett. **67**, 3279 (1991).
[22] M. C. Bartelt and J. W. Evans, Surf. Sci. **314**, L829 (1994).
[23] G. S. Bales and D. C. Chrzan, Phys. Rev. Lett. **74**, 4879 (1995).
[24] A. Pimpinelli, J. Villain and D. E. Wolf, J. Phys. (Paris) **3**, 447 (1993).
[25] H. Röder, K. Bromann, H. Brune and K. Kern, Phys. Rev. Lett. **74**, 3217 (1995).
[26] T. Michely, M. Hohage, M. Bott and G. Comsa, Phys. Rev. Lett. **70**, 3943 (1993).
[27] H. Röder, H. Brune, J. P. Bucher and K. Kern, Surf. Sci. **298**, 121 (1993).
[28] H. Brune, H. Röder, C. Romainczyk, C. Boragno and K. Kern, Appl. Phys. A **60**, 167 (1995).
[29] P. Jensen, A. L. Barabási, H. Larralde, S. Halvin and H. E. Stanley, Nature **368**, 22 (1994).
[30] P. Jensen, A. L. Barabási, H. Larralde, S. Halvin and H. E. Stanley, Phys. Rev. B **50**, 15316 (1994).
[31] L. Bardotti, P. Jensen, A. Hoareau, M. Treilleux and B. Cabaud, Phys. Rev. Lett. **74**, 4694 (1995).
[32] M. C. Bartelt and J. W. Evans, Phys. Rev. B **46**, 12675 (1992).
[33] G. S. Bales and D. C. Chrzan, Phys. Rev. B **50**, 6057 (1994).
[34] J. G. Amar and F. Family, Phys. Rev. Lett. **74**, 2066 (1995).
[35] S. Liu, Z. Zhang, G. Comsa and H. Metiu, Phys. Rev. Lett. **71**, 2967 (1993).
[36] J. Jacobsen, K. W. Jacobsen, P. Stoltze and J. K. Nørskov, Phys. Rev. Lett. **74**, 2295 (1995).
[37] Z. Zhang, X. Chen and M. G. Lagally, Phys. Rev. Lett. **73**, 1829 (1994).
[38] S. C. Wang and G. Ehrlich, Phys. Rev. Lett. **67**, 2509 (1991).
[39] H. Brune, H. Röder, C. Boragno and K. Kern, Phys. Rev. B **49**, 2997 (1994).
[40] J. Kertész and T. Vicsek, J. Phys. A: Math. Gen. **19**, L257 (1986).
[41] During preparation of this manuscript it came to our attention that also Michely et al. interpret their islands as dendritic. They suggest a similar explanation based on anisotropic corner diffusion.
[42] This important difference has first been realized by Zhang et al. in ref. 37
[43] In a former publication (ref. 11) we have suggested that anisotropy in edge diffusion might be responsible for dendritic growth.
[44] T. Michely and G. Comsa, Surface Science **256**, 217 (1991).
[45] K. W. Jacobsen, J. K. Nørskov and M. J. Puska, Phys. Rev. B **35**, 7423 (1987).
[46] P. Stoltze, J. Phys. Condens. Matter **6**, 9495 (1994).
[47] W. W. Mullins and R. F. Sekerka, J. Appl. Phys. A **34**, 323 (1963).
[48] H. Brune, H. Röder, C. Boragno and K. Kern, Phys. Rev. Lett. **73**, 1955 (1994).
[49] H. Brune, K. Bromann, H. Röder, K. Kern, J. Jacobsen, P. Stolze, K. Jacobsen and J. Nørskov, Phys. Rev. B rapid communications in press (1995).